Available online at www.sciencedirect.com
ScienceDirect
Trans. Nonferrous Met. Soc. China 35(2025) 4118−4136
Transactions of Nonferrous Metals Society of China
www.tnmsc.cn

Influence mechanism of reduction rate on interface microstructure and mechanical properties of TA1/TC4 composite plate

Peng ZHANG[1,2,3], Hao ZHAO[2,3,4], Jin-zhou ZHU[1,3,4],
Tao WANG[2,3,4], Zhong-kai REN[2,3,4], Jian-chao HAN[2,3,4], Wen-wen LIU[2,3,4]

1. College of Materials Science and Engineering, Taiyuan University of Technology, Taiyuan 030024, China;
2. National Key Laboratory of Metal Forming Technology and Heavy Equipment, Taiyuan University of Technology, Taiyuan 030024, China;
3. Engineering Research Center of Advanced Metal Composites Forming Technology and Equipment, Ministry of Education, Taiyuan University of Technology, Taiyuan 030024, China;
4. College of Mechanical Engineering, Taiyuan University of Technology, Taiyuan 030024, China

Received 23 August 2024; accepted 28 March 2025

Abstract: The effects of the reduction rate of the corrugated rolling on the microstructure and mechanical properties of TA1/TC4 composite plate that was prepared via corrugated rolling + flat rolling process were investigated. The finite element model was developed and validated for the corrugated rolling process of the composite plate. Experimental findings reveal the absence of significant defects and intermetallic compounds at the bonding interface. When the rolling temperature is 700 °C with the reduction rate of 44% in the first pass of corrugated rolling, the tensile and interfacial shear strengths of the composite plate reach 749 and 403.97 MPa, respectively. The simulation results demonstrate that the plastic strain in the TC4 substrate is enhanced by corrugated rolling and the compressive stress at the trough is high. These results confirm that interfacial bonding is promoted by corrugated rolling, and the mechanical properties of the composite plate are improved significantly with the increase of reduction rate.

Key words: corrugated rolling; TA1/TC4 composite plate; reduction rate; interface microstructure; interface bonding properties

1 Introduction

In light of the inherent limitations of single material in meeting the current industrial requirements for high and comprehensive performance, such as superior mechanical, physical, and thermal properties, composite structures including clad plates and tubes, comprising two or more metals, have been developed and industrialized due to their distinctive and advantageous properties [1,2]. The advantages of these composite structures include the reduction of high-cost metal usage and the enhancement of performance in harsh environments. Pure titanium and titanium alloys are considered valuable strategic resources due to their exceptional properties, such as high specific strength [3], corrosion resistance [4], and high-temperature stability [5]. Meanwhile, they have been widely used in various industries including aviation, aerospace, marine, transportation, and petro-chemicals [6−9]. Due to its excellent comprehensive performance, Ti−6Al−4V (TC4) has already become the most widely utilized titanium alloy. However, the prohibitive cost [10], poor

Corresponding author: Peng ZHANG, Tel: +86-15333016509, E-mail: zhangpeng02@tyut.edu.cn
https://doi.org/10.1016/S1003-6326(25)66933-0

welding performance, and plastic deformation ability are the main reasons for restricting large-scale application for TC4. By contrast, TA1 pure titanium exhibits superior welding performance, excellent ductility, and low density [11], with the cost that is 50%−60% lower than that of TC4. The composite plates made from TC4 and TA1 combine the excellent corrosion resistance and high specific strength of TC4 with the exceptional welding performance and plasticity of TA1. Meanwhile, these composites have significant advantages in terms of cost reduction and lightweight, which can further expand the potential application of titanium alloy. Despite these benefits, research on the manufacturing processes for TC4/TA1 composite plates is still scarce, and published studies on this subject are rare.

At present, common preparation methods of composite plates include the explosive welding [12], extrusion bonding [13], diffusion bonding, and rolling bonding [14−16]. ZHANG et al [17] comprehensively analyzed the influence of diffusion parameters on the shear strength and microstructure evolution of TA1/TC4 dissimilar joints. It showed that the optimum shear strength of 404 MPa was achieved at the temperature of 920 °C with the holding time of 1 h, which not only ensured the comprehensive mechanical properties of the material and the weld but also maintained the high shear strength in the brazing seam. LI et al [18] prepared TC4/TA1/Ti6321 titanium alloy composite plate by explosive welding, achieving excellent bonding between the layers. Among these methods, the rolling composite method stands out due to its advantages of high production efficiency, uncomplicated process, and suitability for large-scale production [19]. However, the traditional flat rolling (FR) method faces a series of challenges, including difficulty in bonding dissimilar substrates, low bonding strength, and poor strip shape quality [20]. Aiming at the problems of FR, the corrugated rolling (CR) process has emerged as the time requires. WANG et al [21] used a new type of corrugated roll/flat roll corrugating rolling and flat roll/flat roll flat rolling to prepare AZ31 Mg/5052 Al composite plate with superior mechanical properties and excellent plate shape. It was found that the CR process could reduce the rolling pressure required for matrixes connection and decrease the residual stress in the composite plate. Besides, for the same reduction, the deformation degree of the substrate material increased with the CR process. In addition, the formation of concave−convex three-dimensional structures leads to an increase in the bonding area at the interface. LIU et al [22] analyzed the CR process of T2 copper and 5052 aluminum alloy composites plate using numerical simulation and studied the deformation behavior. The results showed that the increase of local rolling force promoted the fracture of the surface oxide layer and exposure of fresh metals, which is beneficial to the effective bonding between the substrates.

There are few reports on the preparation of TA1/TC4 composite plates using rolling technology, as most researchers have relied on welding methods to achieve the substrate connection. However, it is difficult to prepare large-size TA1/TC4 composite plates by brazing or diffusion welding. Explosive welding often results in the formation of brittle interfacial compounds, low interfacial bonding strength, and environmental pollution. These limitations hinder the ability of achieving large-scale, continuous production of TA1/TC4 composite plates.

Therefore, in this study, a novel “CR+FR” process is employed initially to fabricate TA1/TC4 composite plates with superior bond strength, outstanding mechanical properties, and excellent plate shape. The influence of the reduction rate during the initial CR stage on the microstructure and mechanical properties of the composite plates is systematically investigated. Furthermore, numerical simulation is conducted to analyze and compare the interfacial stress and strain states, as well as the temperature and velocity field distributions, between the CR and FR processes. And this study provides a theoretical foundation and technical support for the industrial-scale production of large size TA1/TC4 composite plates.

2 Experimental method and finite element model

2.1 Experimental methods

The original experimental materials used in this study were 150 mm × 50 mm × 3 mm TA1 pure titanium plate and 150 mm × 50 mm × 2 mm TC4

titanium alloy plate. The chemical compositions of the TA1 pure titanium plate and TC4 titanium alloy plate used in the experiment are listed in Table 1.

The corrugated hot rolling experiment was implemented in two passes, that was, the first pass used corrugated roll rolling, and the second pass utilized flat roll rolling. The rolling conditions for this experiment were set as shown in Table 2. Earlier experimental results indicated that the elevated temperature softening phenomenon of TA1 became apparent above 700 °C, at which its strength was significantly lower than that of TC4. Higher temperature would lead to a significant $\alpha \rightarrow \beta$ phase transition in the substrate material, thereby degrading its performance. Combined with the actual production experience, the rolling temperature was set as 700 °C. The rolling reduction rates were 26.5%, 35% and 44%, respectively. For the second-pass FR, the temperature and reduction rate were set as 700 °C and 20%, respectively, with the thickness ratio of the TA1 to TC4 substrates being 3:2.

Table 1 Chemical composition of TA1 and TC4 titanium alloys (wt.%)

Alloy	Al	V	Fe	C	N	H	O	Ti
TC4	6.5	4.5	0.3	0.1	0.05	0.015	0.2	Bal.
TA1	−	−	0.25	0.02	0.13	0.004	0.001	Bal.

The first-pass rolling was conducted using a two-roll reversible rolling mill which is equipped with the corrugated top roller and the flat bottom roller to prepare TA1/TC4 composite plate. The corrugated roll had a diameter of 250 mm, the wave number of 140, and the amplitude of 0.75 mm, while the flat roll had a diameter of 250 mm. The edges of the assembly parts were welded to prevent severe oxidation of the bonding surface during the heating process. The rolling process is shown in Fig. 1.

The pre-processed TA1/TC4 assembly parts were placed in a tube furnace with a protective atmosphere. After holding for 20 min, it was taken out and sent to the rolling mill for rolling experiment. During the first pass, the TA1/TC4 composite plate was formed using CR with different

Table 2 Experimental conditions of TA1/TC4 composite plate rolling

Working condition	First-pass rolling		Second-pass rolling		Thickness ratio of TA1 to TC4
	Reduction rate/%	Rolling temperature/°C	Reduction rate/%	Rolling temperature/°C	
a	26.5	700	20	700	3:2
b	35	700	20	700	3:2
c	44	700	20	700	3:2

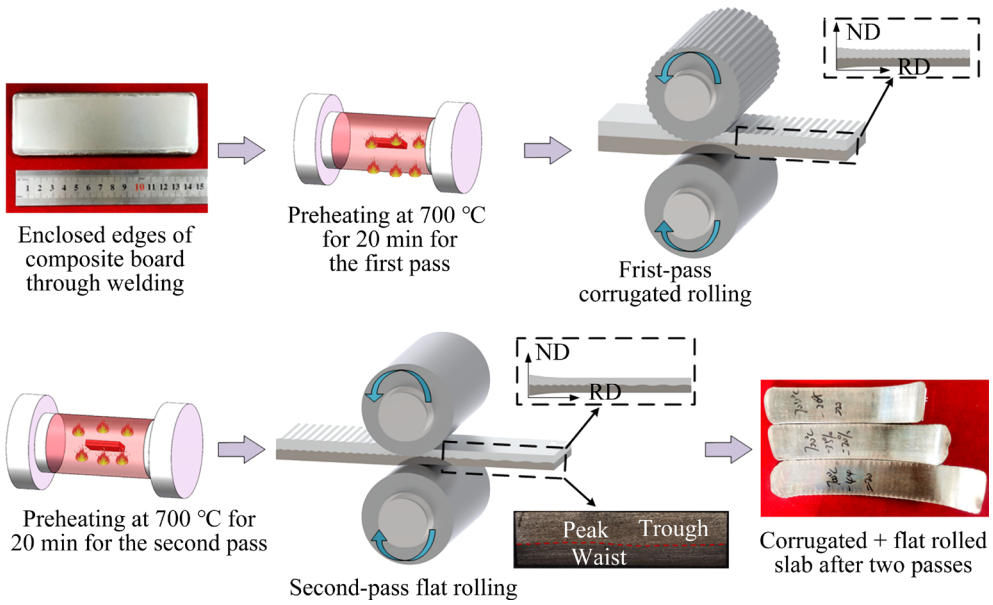

Fig. 1 Schematic of TA1/TC4 composite plate rolling process

reduction rates by adjusting the roll gap, with the TA1 side in contact with the corrugated roll. In the second pass, the plates were produced by FR to improve surface quality and further reduce the thickness of the plates.

The corrugated interface morphology, interface diffusion layer thickness, and defect distribution of the TA1/TC4 composite plate were characterized by scanning electron microscope (SEM) to research microstructure evolution of the interface and the formation of intermetallic compounds (IMCs). The interfacial bonding strength of the TA1/TC4 composite plate was evaluated by tensile and shear tests. The tensile specimens were cut along the rolling direction (RD), while shear specimens were cut along the transverse direction (TD). As shown in Fig. 2, the tensile rates and shear test were conducted at a rate of 0.5 mm/min, and the breakage morphology and element distribution were studied.

2.2 Finite element model construction and verification

DEFORM-3D software was used to simulate the first-pass CR of the composite plate. The true stress−strain curves of TA1 and TC4 are shown in Fig. 3, and the physical properties of TA1 and TC4 are shown in Table 3. The top roller was set as corrugated roll, and the bottom roller was set as flat roll.

Because the deformation of the rollers had negligible effect on the composite plate, the rollers were set as rigid bodies. The welding layer was set between the TA1 and TC4 plates, as shown in Fig. 4, and was bound to both plates. Shear friction was set between the substrates with a friction coefficient of 0.7, while coulomb friction was set between the roller and the substrate with a friction coefficient of 0.35 [23]. The tetrahedral mesh was used with the smallest unit size of 1 mm. In order to be consistent with the experiment, the initial speed

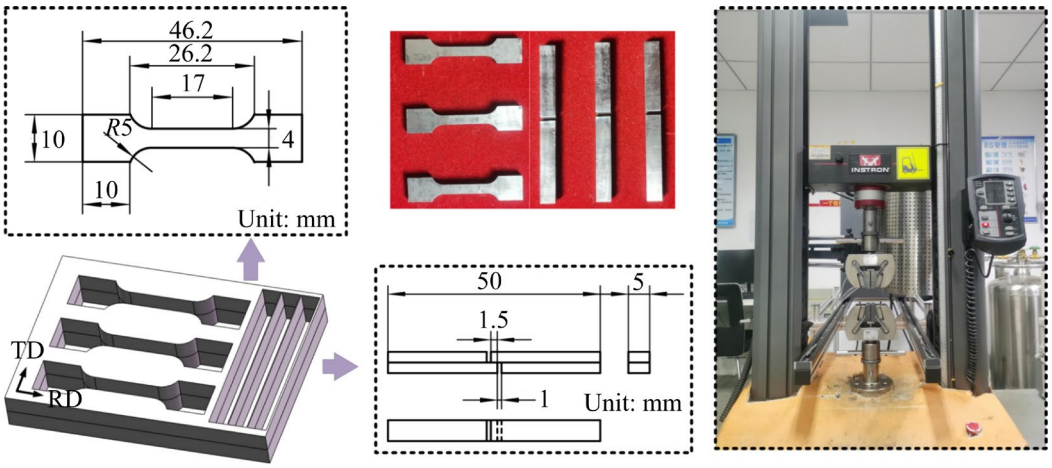

Fig. 2 Schematic of uniaxial tensile and shear samples

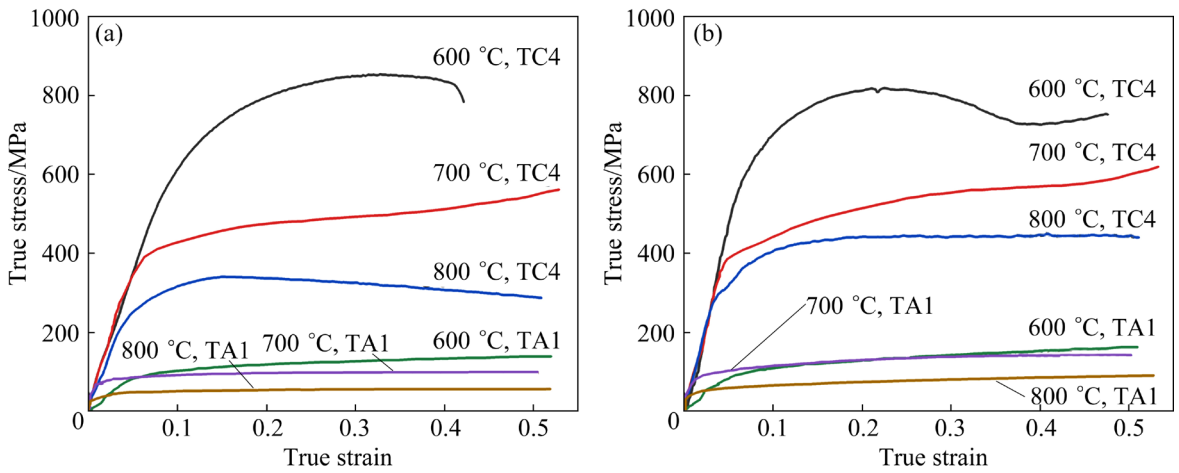

Fig. 3 True stress−strain curves of TA1 and TC4 at different strain rates: (a) 0.1 s^{-1}; (b) 1 s^{-1}

Table 3 Main parameters of TA1 and TC4 (700 °C)

Alloy	Young's modulus/10^4 GPa	Poisson's ratio	Density/ (10^{-9} kg·m^{-3})	Thermal conductivity/ (W·m^{-1}·°C^{-1})	Specific heat capacity/ (J·kg^{-1}·°C^{-1})	Coefficient of thermal expansion/10^{-5} °C^{-1}
TA1	7.53	0.33	4.48	17.84	692	1.03
TC4	7.73	0.34	4.33	13.48	751	1.06

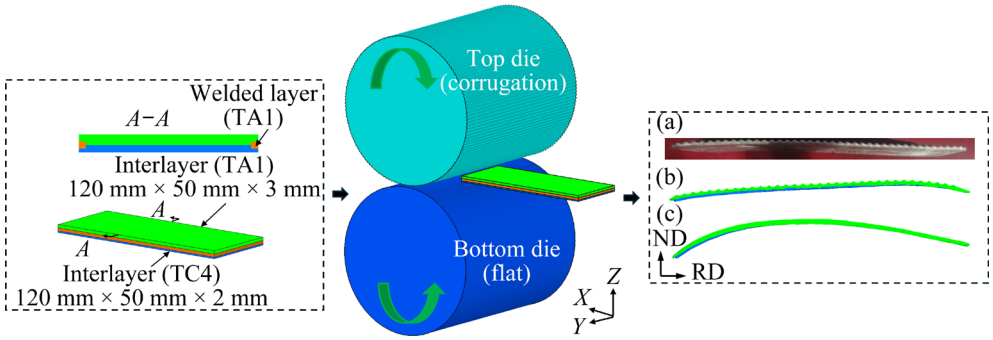

Fig. 4 Construction of finite element model and comparison between experimental and simulation plate shapes of CR

of the plate was set as 100 mm/s before contact with the rollers, and the rolling temperature and rolling speed were set as 700 °C and 122.75 mm/s, respectively. The top roller and bottom roller were set as clockwise rotation and contra rotate, respectively. When the front end of the plate was bitten by the rollers, the initial speed was removed, and the movement of the plate relied on rolling force and friction force.

Figures 4(a) and (b) show the experimental and simulation results of CR, respectively. The plate's shape appears relatively straight, while the TA1 side exhibits corrugation. The degree of material extension on both sides is remarkably close, and the simulation results are consistent with the experimental results. Compared to the simulation results of FR (Fig. 4(c)) with that of CR (Fig. 4(b)), the warping degree of the plate after FR is significantly greater than that of CR. The reason is that CR enhances the extension of the hard material, TC4, in the rolling direction and improves the deformation coordination between TA1 and TC4, resulting in straight plate shape.

3 Results and analysis

3.1 Microstructure and texture of interface

3.1.1 Micromorphology analysis

Figure 5 shows the scanning electron microscope (SEM) characterization results of the interfacial typical position of the TA1/TC4 composite plate under different reduction rates in the first pass. At the first-pass reduction rate of 26.5%, varying degrees of pores are present at the peak, waist, and trough positions of the bonding interface (as shown in the enlarged image in Fig. 1). Additionally, the interface bonding area is relatively small, as depicted in Figs. 5(a_1−a_3). The number and size of pores at these positions are all decreased when the reduction rate is 35%, as shown in Figs. 5(b_1−b_3). There are no obvious pore defects at the trough and waist positions, while only small pores remain at the peak position, indicating a close bond formation when the rate increases to 44%, as shown in Figs. 5(c_1−c_3).

Based on the observed phenomena, it can be seen that with the increase of the first-pass reduction rate, the interface defects of the composite plate were gradually decreased, and the state of interface bonding continues to improve. It shows that, within the 44% reduction rate, the increase of the reduction rate is beneficial for the bonding of the composite plates. Under high magnification, the CR interface exhibits an undulating morphology. The reason is that in the severe local loading conditions from the corrugated roller, the softer TA1 metal penetrates the dense oxide layers on the surfaces of both plates and squeeze into the TC4 side. This process facilitates the tight bonding of fresh metal from both substrates, consistent with the theory of metal composite plate crack bonding [24].

Figure 6 shows the energy dispersive spectrometer (EDS) line scanning results of the typical

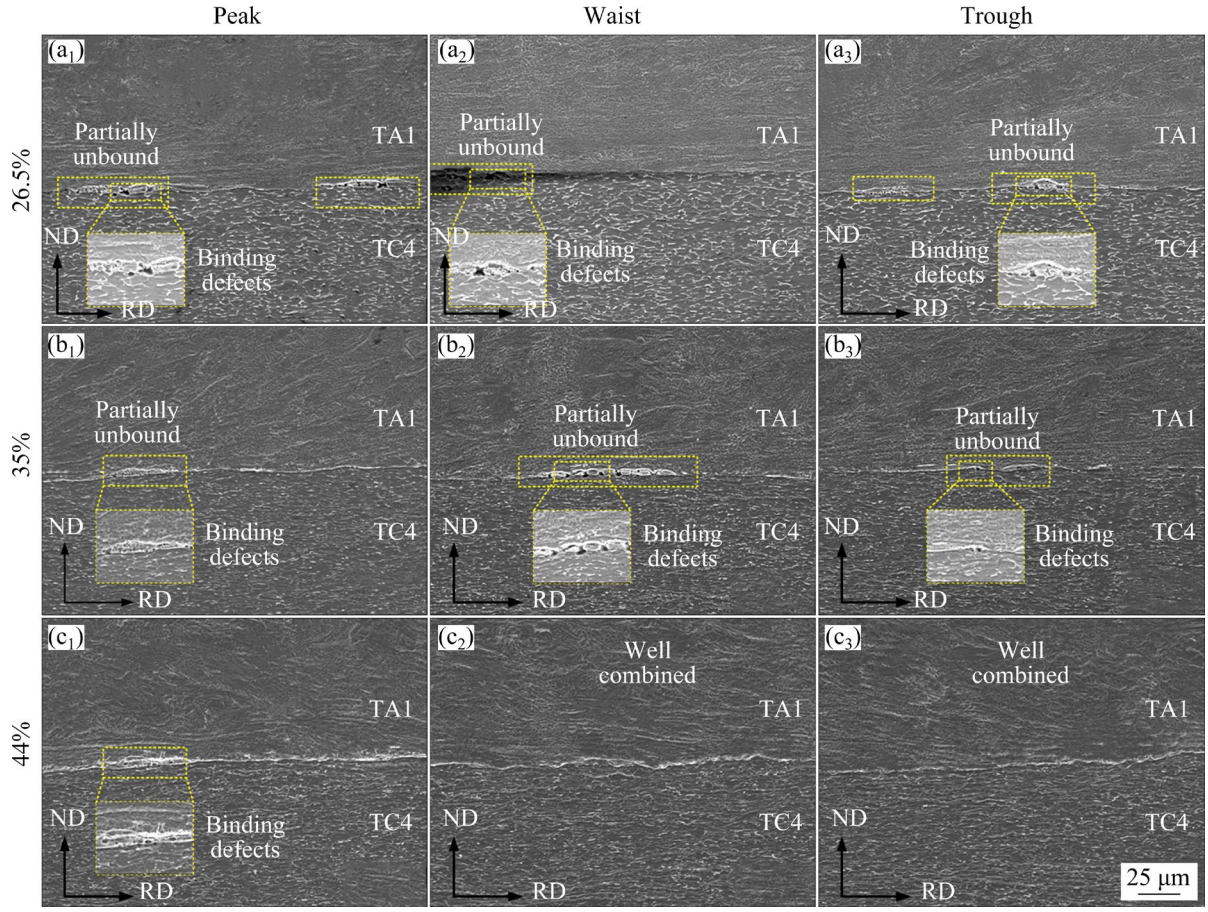

Fig. 5 Interfacial SEM characterization results of composite plates at different reduction rates in the first pass at 700 °C

position of the TA1/TC4 composite plate. The distribution trends of Ti and Al elements at the interface exhibit X-shaped without platform characteristics, indicating the absence of IMCs at the interface. The composite structure results from mechanical interlocking and metallurgical bonding due to element diffusion, which enhances the bonding performance [25]. It can be seen from Fig. 6 that when the reduction rate increases from 26.5% to 35%, the thickness of the diffusion layer at the interface of the composite plate has no evident change. However, when the reduction rate reaches 44%, the thickness of the diffusion layer becomes thinner compared to that at 35%. It can be observed that as the reduction rate increases, the thickness of the diffusion layer in the TA1/TC4 composite plate decreases once a certain reduction rate is reached. The reason is that the substantial reduction rate leads to severe plastic deformation of the diffusion layer and then thinning. Besides, the diffusion layer primarily consists of a solid solution formed by the diffusion of aluminum from the TC4 side to the TA1 side, as shown in Fig. 6.

3.1.2 Microstructure and texture evolution analysis

The research shows that the plastic deformation at the trough of the interface is severe, and the microstructures at the typical position are similar. The microstructure characteristics and evolution law at the trough of the bonding interface are analyzed by electron back scatter diffraction (EBSD). Figure 7 shows the orientation distribution map and kernel average misorientation (KAM) diagram at the trough of the interface in the conditions of minimum (26.5%) and maximum (44%) reduction rates, respectively.

As shown in Figs. 7(a, b), at the reduction rate of 26.5%, the grain size on the TC4 side is significantly different. Elongated deformation grains along the RD dominate, within which there are a large number of small-angle grain boundaries and dislocation cells. The average grain sizes along the RD and normal direction (ND) are 6.88 and 2.44 μm, respectively. Equiaxial grains with an average size of 1.5 μm are observed between the large deformed grains. Besides, a large amount of fine and uniform equiaxial grains, resulting from

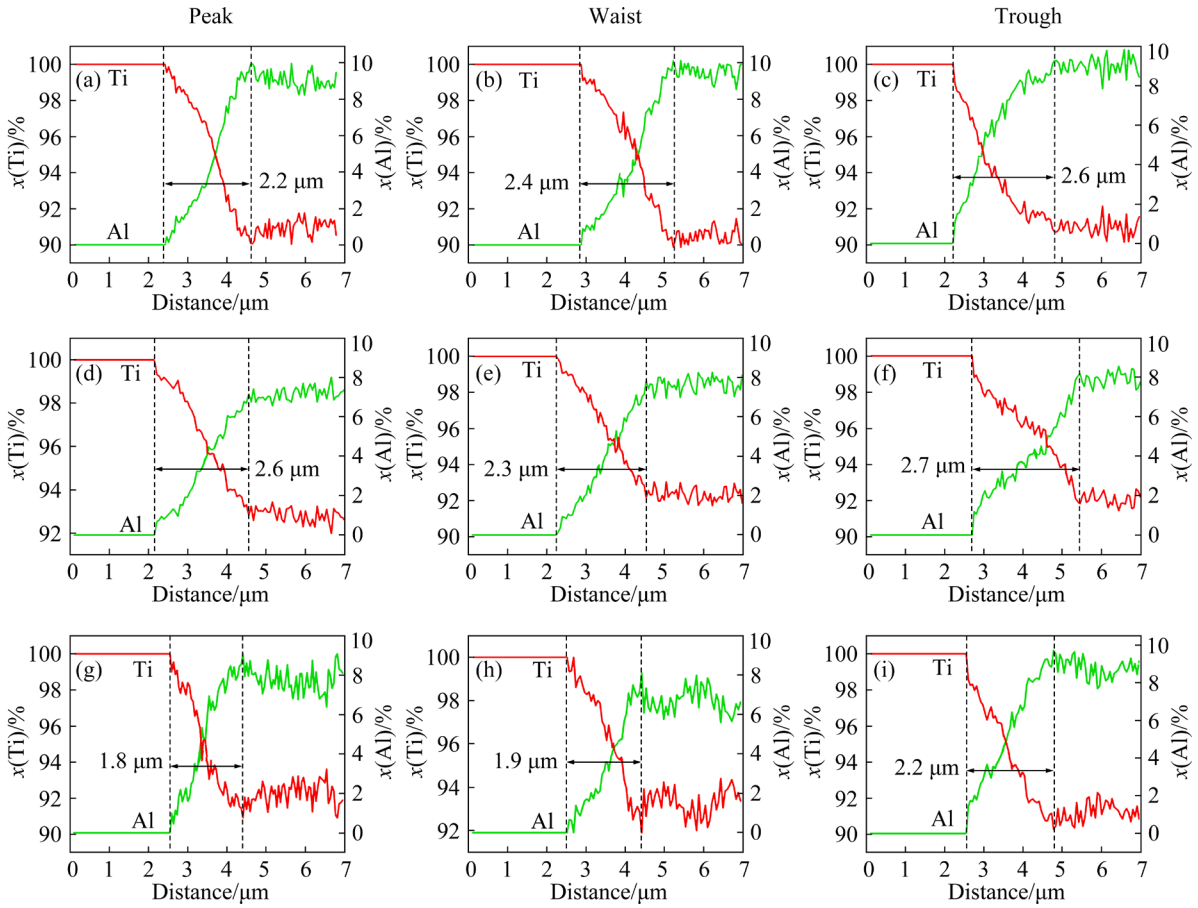

Fig. 6 EDS line scan results of interface of composite plate at different reduction rates for the first pass at 700 °C: (a−c) 26.5%; (d−f) 35%; (g−i) 44%

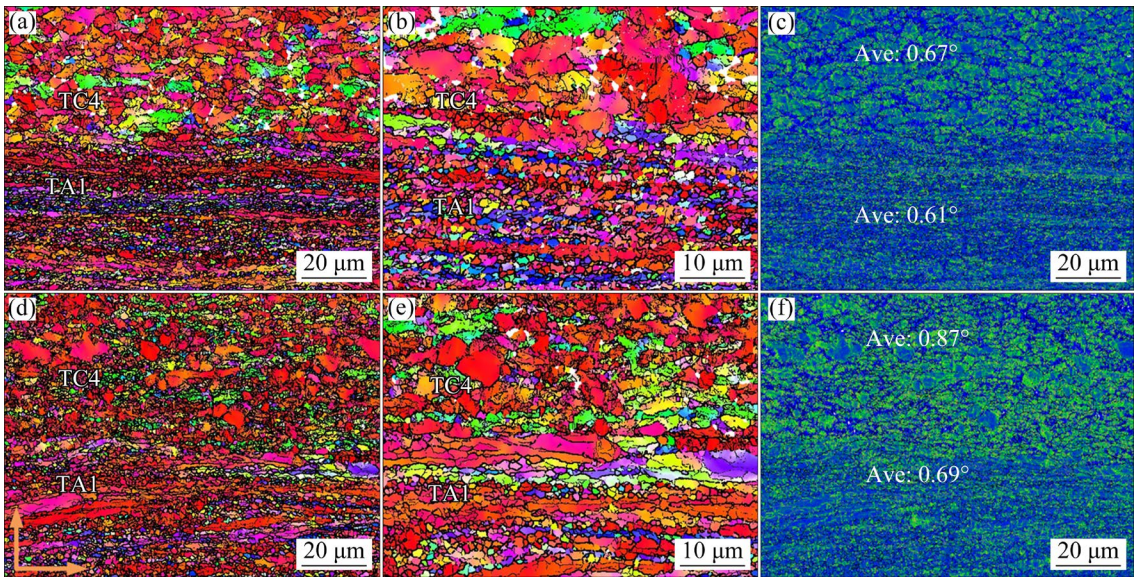

Fig. 7 EBSD analysis results of interface for TA1/TC4 composite plate: (a, b) Orientation maps at reduction rate of 26.5%; (c) KAM distribution at reduction rate of 26.5%; (d, e) Orientation maps at reduction rate of 44%; (f) KAM distribution at reduction rate of 44%

the fragmentation of elongated deformed grains, are distributed along the RD on the TA1 side, with an average grain size of 0.75 μm. It can be seen that the proportion of deformed grains is the highest in both substrates. Most substructures are distributed on the TC4 side, while part of dynamic

recrystallization occurs on the TA1 side. Almost no twin crystals are present in either substrate, as twins are broken and subgrain boundaries are formed during hot rolling [26].

KAM presents the local dislocation density and internal strain distribution of the material by measuring the orientation deviation between a point and a surrounding point [27]. It can be seen from Fig. 7(c) that the KAM values of 0.67° and 0.87° on the TC4 side are higher than those of 0.61° and 0.69° on the TA1 side at the reduction rates of 26.5% and 44%, respectively, which demonstrates that a large number of substructures and dislocations are distributed inside the large-size grains on the TC4 side. The reason for this phenomenon is that during the transfer of the plates from the heating furnace to the rolling mill, the actual rolling temperature is lower than 700 °C due to thermal convection and heat conduction, which is significantly lower than the recrystallization temperature of TC4. At the reduction rate of 26.5%, a large number of grains on the TC4 side undergo plastic deformation, and the density of geometrically necessary dislocations (GNDs) increases significantly. However, the degree of dynamic recovery is low, resulting in the retention of a large number of sub-structure. Additionally, it is observed that dislocation density increases on both the TC4 and TA1 sides with the increase of reduction rate, with the increment being more pronounced on the TC4 side. This suggests that the material deformation is exacerbated with the increase of reduction rate, which primarily occurs on the TC4 side. At the same time, due to the low recrystallization temperature of TA1 and the severe plastic deformation, the dynamic recrystallization grains form with the decrease of dislocation and substructure. In addition, because the rolling temperature lies in the α single-phase region, the content of the β-phase on the TC4 side is low, and the α-phase is the main phase.

As shown in Figs. 7(d, e), the grain size of the TC4 side decreases significantly with the increase of reduction rate, showing a mixed distribution of equiaxed grains with varied sizes. The average sizes are 5.32 and 1.2 μm, corresponding to large-size and small-size equiaxed grains, respectively. The large-sized elongated grains are concentrated at the interface, and the gradient distribution of fine grains and large-sized grains imparts both high strength and high toughness to the material. The difference in grain size on the TA1 side becomes more pronounced, with the grains primarily consisting of fine equiaxed grains distributed along the RD. In addition, the grains are predominantly fine and equiaxed, distributed along the RD.

With the increase of reduction rate, the degree of uneven deformation inside TA1 increases, which is related to the aggravation of local strain caused by CR and the nonuniformity of overall deformation [28]. Compared with Figs. 7(c) and (f), the dislocation density on the TA1 side is decreased and that on the TC4 side is enhanced when the reduction rate is 44%. This indicates that the increase in reduction rate causes only slight deformation of the TA1 side, but significantly great deformation of the TC4 side. The increase of deformation results in grain refinement, proliferation, and entanglement of dislocations, with a pronounced work hardening effect. At the same time, the matrix exhibits obvious dislocation and fine grain strengthening, which improves the strength of the composite plate [29] but reduces its toughness and plasticity, consistent with the tensile test results.

Figure 8 presents the recrystallization and grain boundary distribution maps at the trough of the composite plate under the conditions of minimum and maximum reduction rates. The recrystallization distribution figures show the distribution of recrystallized grains (blue), sub-grains (yellow), and deformed grains (red). Figure 8(c) shows the corresponding statistical results. It can be seen from Figs. 8(a, b) that recrystallized grains are mainly distributed on the TA1 side, but less on the TC4 side. When the reduction rate is 26.5%, the recrystallization ratios of the TA1 and TC4 sides are 15% and 3%, respectively. The reason is that deformation during rolling primarily occurs on the TA1 side, and the dislocation density is increased by the accumulation of strain, which in turn promotes the dynamic recrystallization of the material [30].

Figures 8(d, e) are grain boundary maps, where the green lines and black lines are high angle grain boundaries (HAGBs >15°) and low angle grain boundaries (LAGBs, 2°−15°), respectively. Figure 8(e) provides a statistical map of the proportion of LAGBs and HAGBs, which characterizes the level of grain deformation and internal dislocation density [31]. Figure 8(f) shows that when the reduction rate is 26.5%, the

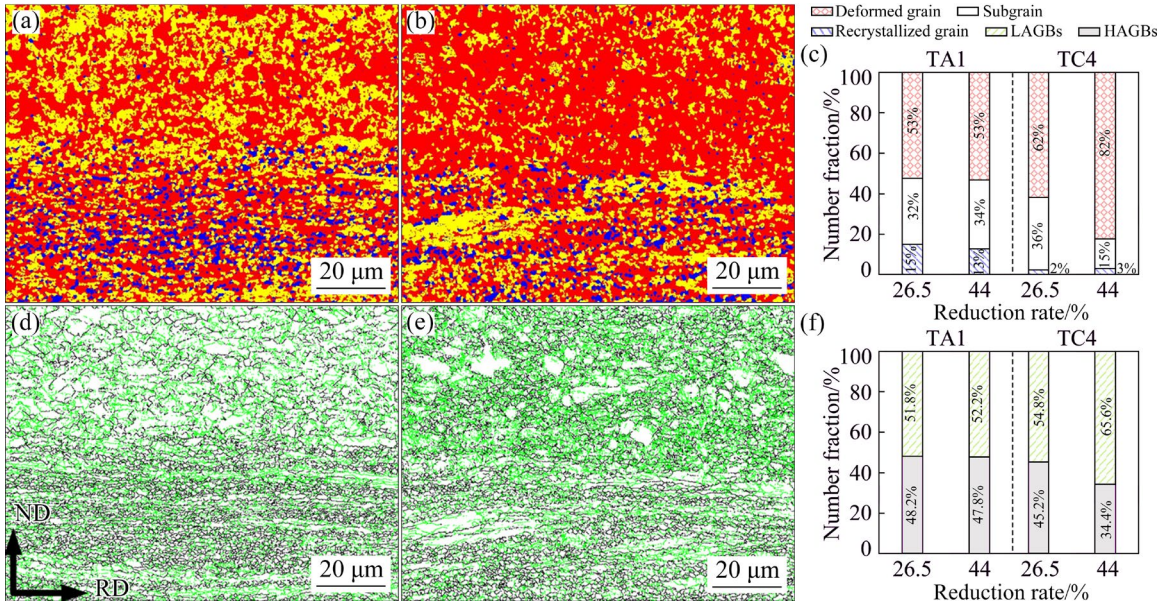

Fig. 8 EBSD analysis results of interface for TA1/TC4 composite plate: (a, b) Recrystallization grain distribution maps at reduction rates of 26.5% and 44%, respectively; (c) Recrystallization distribution histogram; (d, e) Grain boundary distribution maps at reduction rates of 26.5% and 44%, respectively; (f) Grain boundary distribution histogram

proportions of LAGBs on the TA1 and TC4 sides are 51.8% and 54.8%, respectively. When the reduction rate is increased to 44%, the proportions of LAGBs on the TA1 and TC4 sides are 52.2% and 65.6%, respectively. It reveals that with the increase of reduction rate, the proportion of LAGBs on the TA1 side changes minimally, while the proportion of LAGBs on the TC4 side increases remarkably. This is because when the reduction rate reaches 26.5%, the grain deformation of TA1 becomes exceptionally pronounced, and the work hardening effect is significant. As a result, further plastic deformation primarily occurs on the TC4 side. Furthermore, as the reduction rate increases, while dislocation density and the number of deformed grains increase, the recrystallized domains exhibit no substantial expansion. Consequently, the deceleration in the transformation of LAGBs to HAGBs, resulting in elevated fraction of LAGBs. At this time, the grains on the TA1 side are nearly no longer refined with the increase of the reduction rate, while both the dislocation density and the LAGBs demonstrate only marginal variations.

Figure 9 shows the polar figure and inverse pole figure (IPF) at the trough of the bonding interface by "CR + FR". There are two phases consisting of α and β in TC4 titanium alloy, but the content of the β phase is low after hot rolling at 700 °C. Therefore, the texture evolution analysis focuses primarily on the α phase rather than the β phase. When the reduction rate is 26.5%, the corresponding polar figure and IPF on the TC4 side are shown in Fig. 9(a). It is shown that the orientation of ⟨0001⟩//TD, exhibiting a maximum pole density of 8.67, demonstrates 10°−30° tilt toward the ND with scattering along the RD, characteristic of the typical bimodal basal T-type texture in TC4 titanium alloy [32]. The pole figure of the $(10\bar{1}0)$ crystal plane indicates the presence of low-intensity $\langle 10\bar{1}0\rangle$//ND and $\langle 10\bar{1}0\rangle$//RD orientations. Moreover, the IPF analysis confirms a pronounced ⟨0001⟩//TD texture on the TC4 side. In contrast, as shown in Fig. 9(b), the maximum pole density on the TA1 side reaches 15.69, primarily characterized by ⟨0001⟩//ND orientation, with 30°−60° deflection toward the TD, forming a typical basal-tilted texture. Additionally, the $\langle \bar{1}2\bar{1}0\rangle$//RD texture with pole density of 7.62 is present on the TA1 side.

When the reduction rate reaches 44%, there is a slight decrease in the texture strength of the TC4 side. Analysis of the (0001) pole figure reveals that the texture remains dominated by a bimodal T-type pattern. However, the crystallographic *c*-axis shows a more pronounced inclination toward the ND, while the inclination toward the RD is reduced. The

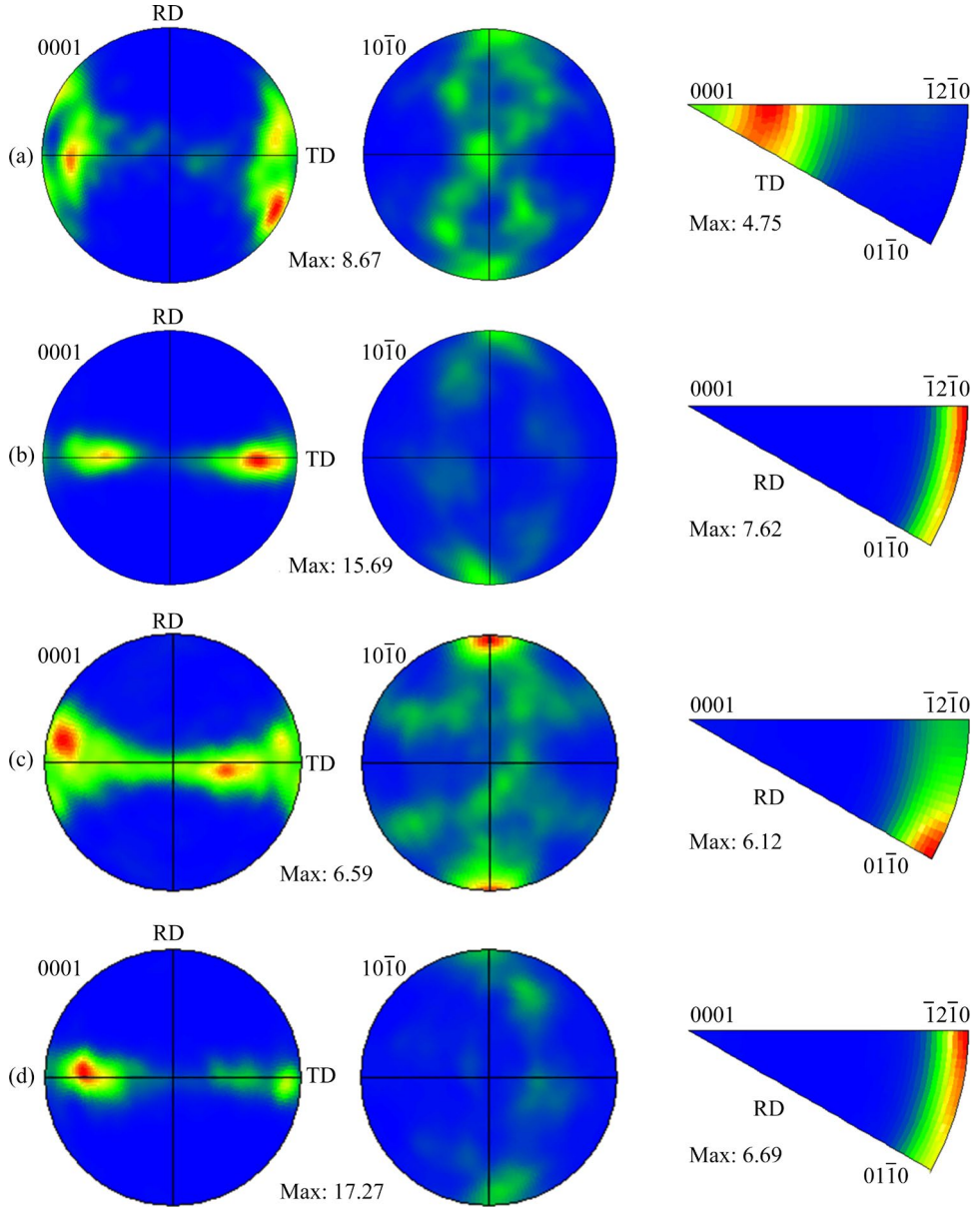

Fig. 9 Polar figure and IPF of TA1/TC4 composite plate at different reduction rates: (a) 26.5%, TC4 side; (b) 26.5%, TA1 side; (c) 44%, TC4 side; (d) 44%, TA1 side

$(10\bar{1}0)$ polar figure and IPF indicate a gradual enhancement in the texture strength of $\langle 10\bar{1}0\rangle$//RD, showing a deformed state. For the TA1 side, the texture type remains essentially unchanged, but the texture strength is increased to 17.27, continuing to be dominated by the basal-tilted texture. Under this rolling condition, cylindrical $\langle a\rangle$ slip and basal $\langle a\rangle$ slip mainly occur on both matrixes.

3.2 Interface stress and material deformation mechanism of composite plate

Figure 10 presents the simulation results of the compressive stress and equivalent strain of TA1/TC4 clad plate prepared by FR and CR, respectively, when the reduction rate is 44%. As previously mentioned, higher compressive stress at the bonding interface facilitates the breaking of the oxide layer, allowing fresh metal from the softer side to be squeezed into the harder side. This results in the formation of the mechanical interlocking and element-diffusion-driven metallurgical bond [33,34]. Comparing Figs. 10(a−c), the compressive stress ranges from 989 to 1115 MPa at the peak and from 1168 to 1349 MPa at the trough, with the compressive stress at the trough exceeding that at the peak. By contrast, Fig. 10(c) shows that the range of compressive stress component at the FR

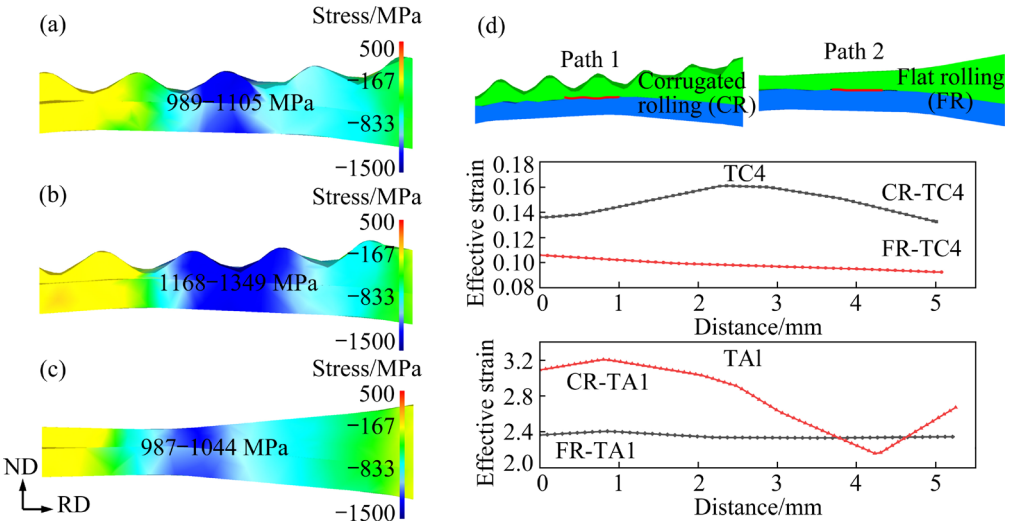

Fig. 10 Simulation results of CR and FR TA1/TC4 composite plates (reduction rate of 44%) and normal stress component distribution map: (a) Peak; (b) Trough; (c) FR; (d) Interface equivalent strain distribution

interface is from 987 to 1044 MPa under the same reduction rate. The results show that the compressive stress at the CR interface is significantly higher than that observed at the FR interface.

Additionally, the increased equivalent strain in the hard metal (TC4) near the interface leads to the more significant fracture of the oxide layer, thereby enhancing the bonding. Meanwhile, the uneven distribution of equivalent strain in the soft metal (TA1) further contributes to the bonding process. Figure 10(d) shows the interfacial equivalent strain distribution for the CR TA1/TC4 composite plate corresponding to Path 1 and that for FR corresponding to Path 2. As shown in Fig. 10(d), it can be seen that the equivalent strain in the TA1 side is higher than that of TC4. This observation can be attributed to the higher strength of TC4 compared to TA1 at the same temperature, making it more difficult for the material to undergo plastic deformation. The equivalent strain of the TC4 side corresponding to the CR process is higher than that of the FR process. Furthermore, the equivalent strain at the peak position on the TA1 side during the CR process is lower than that at the trough position, indicating uneven deformation. Additionally, the equivalent strain at the peak is slightly lower than that observed during the FR process.

The results show that the CR process results in a high equivalent plastic strain near the interface of the hard side metal (TC4), which is beneficial for the broken interface oxide layer. In contrast, the equivalent plastic strain distribution within the softer metal (TA1) is not uniform, leading to the increase of deformation storage energy and promotes the diffusion of elements [35], thereby improving the combination of both substrates.

Figure 11(a) shows the temperature field distribution during the CR process. It can be seen that the surface temperature near the roll is the lowest, which is due to heat transfer between the plate and the rolls. The temperature exhibits a gradient distribution along the normal direction and decreases from the interior to the surface. At the same time, the temperatures at the roll entry and at the interface of the plate are higher than the initial temperature of the plate, which is caused by the conversion of plastic deformation energy into heat energy. It can be seen that the overall temperature is lower than the temperature of the β single-phase region of TC4 [36] and the β-phase transition temperature (882 °C) of TA1 [37]. This condition helps avoid the formation of large β-phase in the composite slab, thereby reducing the potential negative impact on mechanical performance. Figure 11(b) presents the temperature field distribution map during the FR process. The overall temperature presents gradient distribution, with the interface temperature exceeding the initial temperature of the plate. Similar to the CR process, the overall temperature in the FR process is also lower than the phase transition temperature from α phase to β phase.

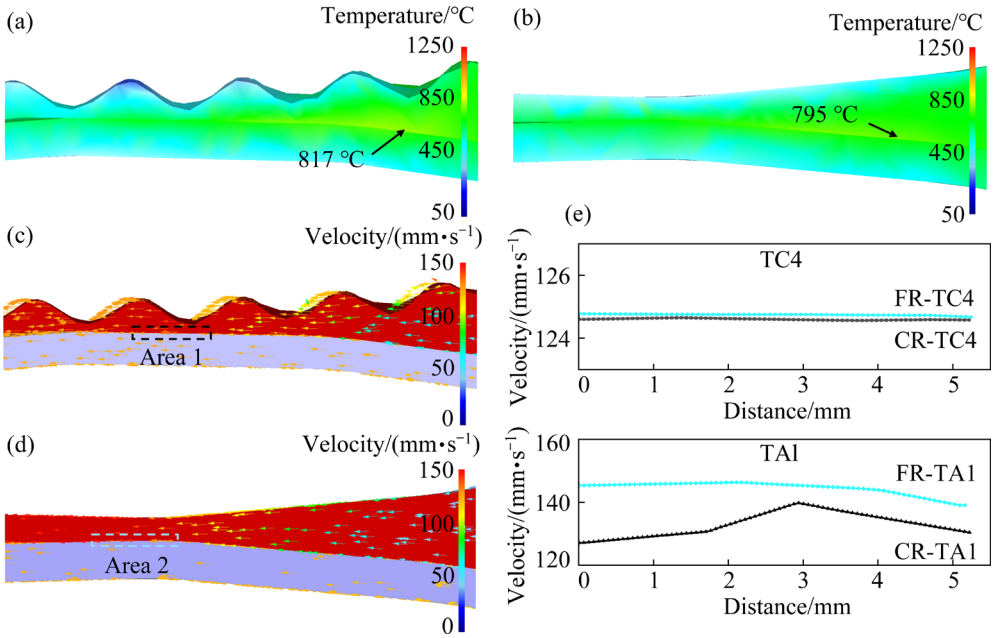

Fig. 11 Temperature fields (a, b) and velocity distribution (c, d) of TA1/TC4 composite plate (reduction rate of 44%): (a, c) CR; (b, d) FR; (e) Interface velocity distribution

Figures 11(c, d) depict the velocity vector figures during the CR and FR processes. It can be seen that the flow speed of materials in the back slip zone is improved. The instantaneous flow direction of the material on the surface aligns with the rolling direction, while internally, the material flows both toward the interface and along the rolling direction. This indicates that the material also moves in the thickness direction, resulting in thin final thickness. When the plate enters the forward slip zone, the material's movement speed increases to match the roll speed, causing elongation and deformation. Figure 11(e) shows the interfacial velocity distribution of the CR TA1/TC4 composite plate corresponding to Area 1 and that of FR corresponding to Area 2. It illustrates that the velocity on the TA1 side during CR is lower compared to FR, whereas the difference on the TC4 side is negligible. This indicates that corrugated rolling effectively reduces deformation on the softer metal, promoting deformation coordination of the material on both sides. Furthermore, within the deformation zone, the relative velocity of the material on both sides during CR is lower than that during FR. A relative low velocity enhances the bonding quality. These findings demonstrate that CR promotes better deformation coordination and stronger interfacial bonding.

The numerical simulation results show that the CR process generates the highest compressive stress at the trough of the interface. Compared to the FR process, the CR process facilitates the penetration of the oxide layer by the softer metal (TA1), allowing it to bond more effectively the harder metal. Meanwhile, the CR process increases the strain degree of the harder material and induces uneven strain in the softer metal, which is beneficial for the tearing of oxide layer and improves the combination and deformation coordination of the materials in both substrates. In addition, the processes of CR and FR at 700 °C effectively avoid the formation of large β phase which reduces mechanical properties.

3.3 Mechanical properties of composite plate

3.3.1 Tensile performance

The influence of reduction rates on the tensile performance of the composite plate was studied. Figure 12 presents the tensile stress−strain curves of the TA1/TC4 composite plate following two-pass rolling, with varying reduction rates applied during the first pass. It can be seen from Fig. 12 that the reduction rate has significant effects on the tensile strength of the composite plate and the elongation of both substrates. When the reduction rate is 26.5%, the tensile strength of the composite plate is

710.93 MPa, with the elongation of the TC4 side is about 11.2% and the elongation of the TA1 side is about 16%. The deformation degree of both substrates is obviously uncoordinated.

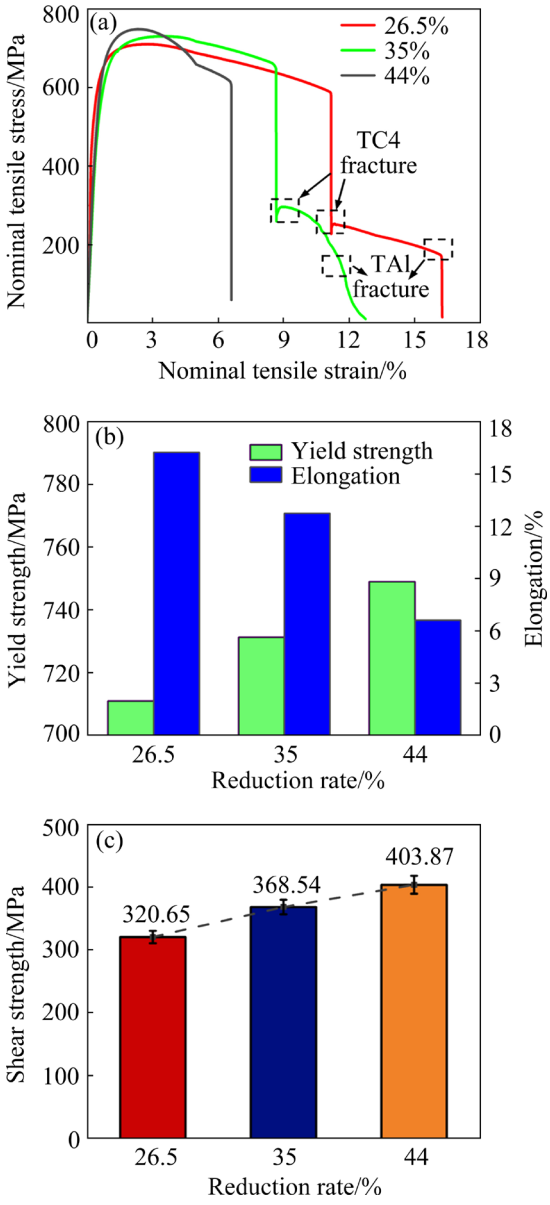

Fig. 12 Mechanical properties of TA1/TC4 composite plate: (a) Tensile stress−strain curve; (b) Tensile properties; (c) Tensile−shear performance

As shown in Fig. 12(a), the tensile curve shows two bends in the fracture part, corresponding to the rupture of the TC4 matrix and the TA1 matrix in the composite plate. When the reduction rate reaches 44%, the tensile strength of the composite plate reaches the maximum of 729 MPa, but the elongation of the composite plate decreases obviously to about 6.2%. At the same time, the deformation of both substrates becomes more coordinated. The main reason is that the composite plate has significant work hardening, particularly on the TA1 side, at high reduction rate. As a result, the strength of the composite plate increases, but the toughness and plasticity decrease significantly.

In order to study the effect of reduction rate on interfacial fracture characteristics, the tensile fracture surfaces were analyzed, as shown in Fig. 13, with TC4 on the top side. Based on the comparisons of macroscopic morphology, it can be seen that with the increase of the reduction rate, the interface crack of the tensile fracture is obviously small, which shows that the bonding strength of the composite plate is gradually increased. Notably, the TA1 side demonstrates superior ductility compared with the TC4 side, exhibiting more pronounced plastic deformation during fracture.

When the reduction rate is 26.5%, there is a certain degree of necking in the rupture deformation area on both the TA1 and TC4 sides. The fracture mode exhibits characteristic toughness breakage, with fibrous at the macroscopic and honeycomb at the microscopic. The toughness and plasticity of the materials in both substrates significantly deteriorate under the gradual increase of the reduction rate, resulting in a pronounced reduction in the necking observed at the fracture, which is consistent with the tensile test results. The size and depth of the dimples can reflect the plastic deformation ability of the material. When the reduction rate is 26.5%, there are large dimple size and depth, with reduced core position of the holes formed by the fracture, which indicates better plasticity and elongation of the material. Microstructure of tensile fractures at reduction rate of 26.5% indicates the predominance of large and deep dimples with few equiaxed dimple present on both TA1 and TC4 sides.

With the increase of the reduction rate, the dimples gradually diminish in size and depth while their number significantly increases, indicating reduced plasticity, especially on the TC4 side. When the reduction rate is 44%, tearing ridges appear at multiple positions on the TC4 side, and the macroscopic morphology of part of the surface becomes relatively flat, exhibiting characteristics of brittle fracture. Compared with the rupture characteristics observed at low reduction rates, the dimples on the TA1 side decrease in size, reflecting reduction in the plastic deformation capability. The

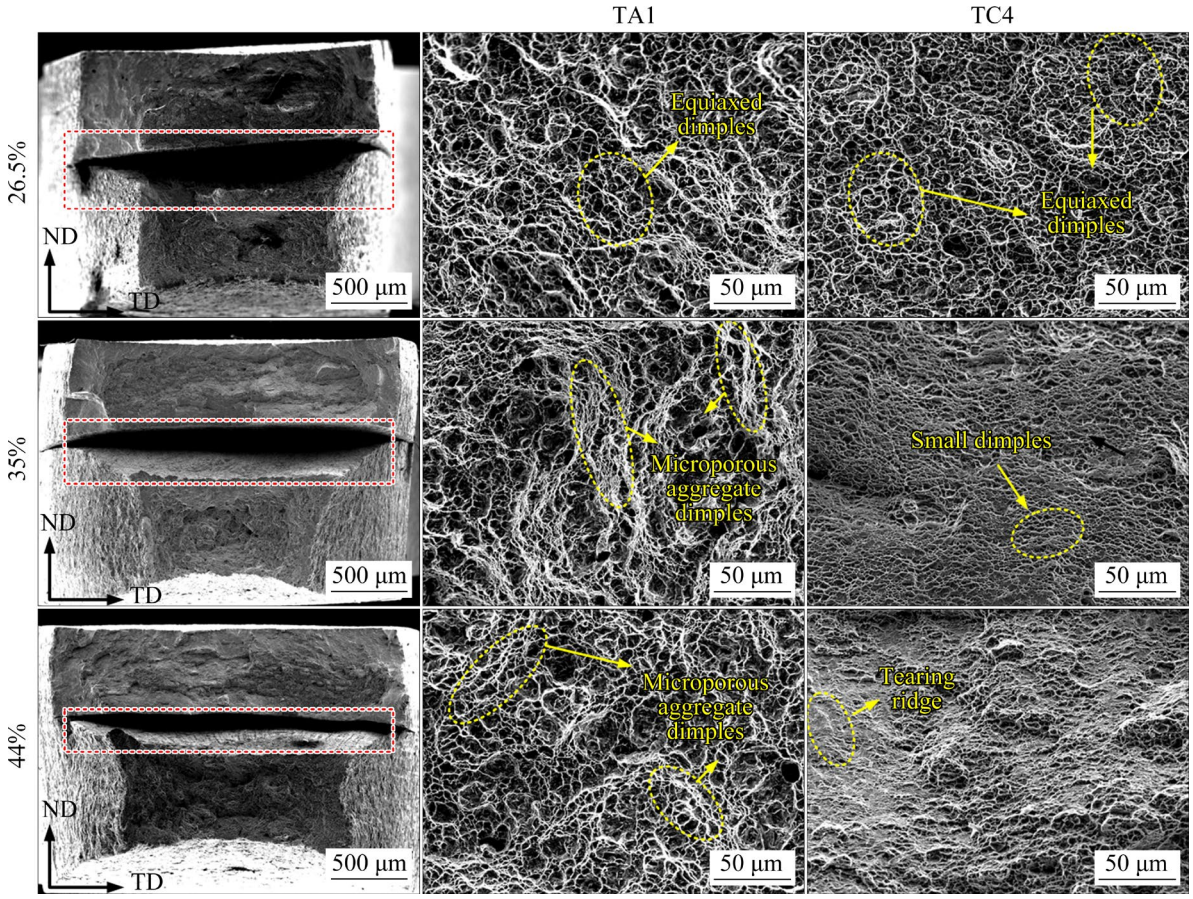

Fig. 13 Tensile fracture morphology of composite plate under different reduction rates at 700 °C in the first pass

results show that with the increase of the reduction rate, the plasticity of the composite plate worsens, leading to gradual reduction of the gaps at the interface for the tensile fracture. Besides, at the reduction rate of 44%, the number of dimples on both sides is gradually low, with the TC4 side presenting brittle breakage characteristics. The fracture mode of the composite plate gradually changes from ductile fracture to brittle fracture.

3.3.2 Shear resistance

The effect of reduction rates in the first pass on the interfacial bonding strength of the composite plate after "CR + FR" rolling is shown in Fig. 12(c). The interfacial shear strength of the TA1/TC4 composite plate is proportional to the reduction rate. When the reduction rate varies from 26.5% to 44%, the shear strength of the composite plate increases significantly from 320.65 to 403.87 MPa.

Figure 14 shows the microscopic morphology of the shear rupture and the results of EDS scanning distribution. Because Al and V elements exist in TC4 alloy, which are absent in the TA1 pure titanium, the elements including Ti, Al, and V are selected for surface scanning. The scanning results indicate that the TA1 side contains a small amount of Al element, which is due to the diffusion of Al element from the TC4 side to the TA1 side. The proportion of the elements on shear fracture surfaces is shown in Table 4.

As shown in Figs. 14(a) and (a_1), at the reduction rate of 26.5%, a large amount of shear dimples and localized shear fractures with white tearing ridges are distributed on the fracture surfaces of both TC4 and TA1 sides. Obvious micropore aggregation fracture is shown by the dimples, and the interface shear rupture mode is still dominated by ductile fracture. As shown in Table 4, the proportion of Ti element at the interface is found to be 99.7%, indicating that the shear breakage is located in the TA1 matrix. The reason for the formation of these bright white small dimples is mainly that the TA1 matrix has better plasticity and lower strength under this rolling condition. In addition, partial slip flat areas are present on both fracture surfaces which are considered typical brittle rupture feature. The stress

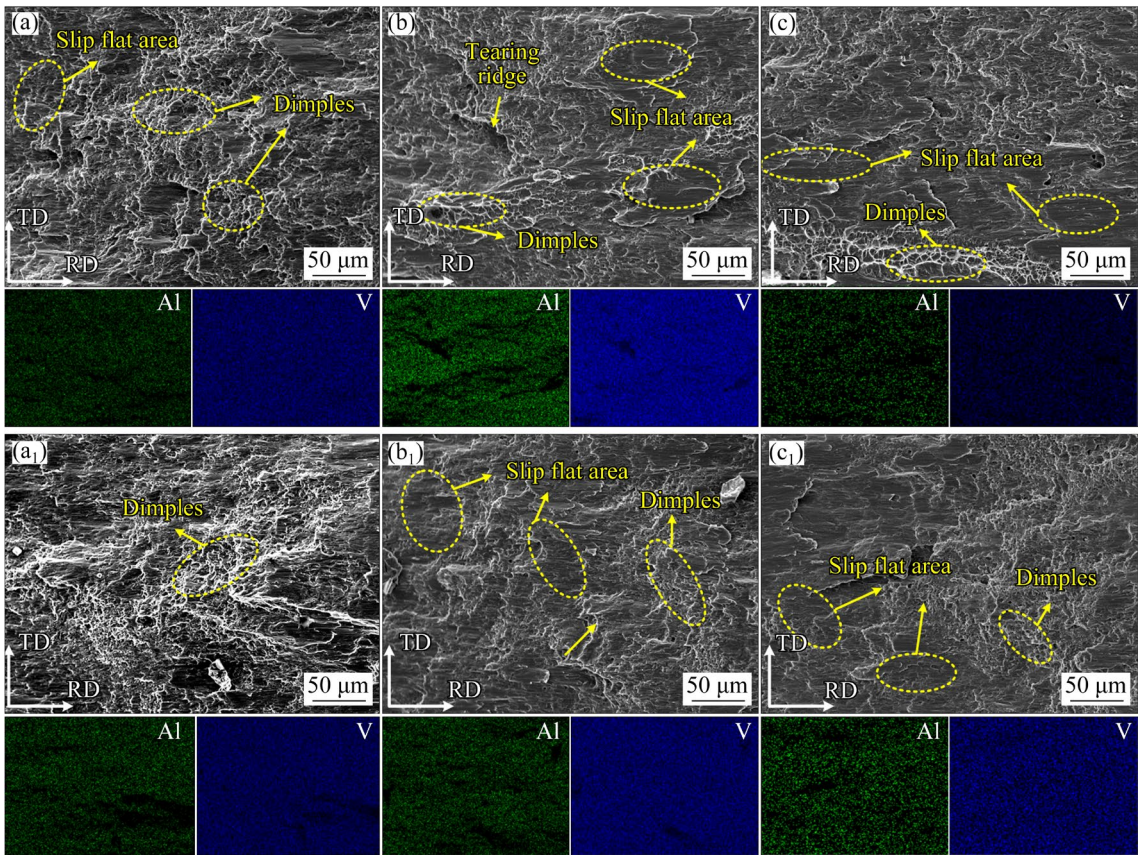

Fig. 14 Shear fracture morphology and EDS mapping images of composite plates at different compression rates for the first pass: (a, a_1) 26.5%; (b, b_1) 35%; (c, c_1) 44%; (a−c) TC4; (a_1−c_1) TAl

Table 4 Element composition at shear fracture of TA1/TC4 composite plate (at.%)

Condition	TC4 side			TA1 side		
	Ti	Al	V	Ti	Al	V
a	99.7	0.2	0.1	99.8	0.1	0.1
b	99.8	0.1	0.1	99.7	0.3	0
c	99.9	0.1	0	100	0	0

concentration in partial areas of the TA1 side after rolling promotes brittle fracture of the material under shear stress, resulting in separation on the TA1 side. This shows that the interface bonding strength of the TA1/TC4 composite plate under this working condition is governed by the shear strength of the TA1 matrix.

At the reduction rate of 35%, as shown in Table 4, there is no significant raising in the content of Al and V elements at the interface, which indicates that shear fracture is still located in the TA1 matrix. Some dimple aggregations are still present in the rupture, but the characteristics of shear dimples are less pronounced, while the proportion of slip flat area increases. Other, the breakage pattern of both substrates is still dominated by ductile fracture, as shown in Figs. 14(b) and (b_1). The reason is that with the increase of the reduction rate, the dislocation density in both matrixes is increased, the work hardening phenomenon is intensified, and the shear strength of the composite plate is further enhanced. As shown in Figs. 14(c) and (c_1), at the reduction rate of 44%, the strength of substrates on both sides further increases, and pure shear fracture with relatively flat morphology is presented. Besides, part of the breakage position is occupied by the slip flat zones, which indicates that the breakage mode is transformed into brittle fracture.

As shown in Table 4, the negligible change in element content indicates that shear fracture still takes place in the TA1 matrix. The results show that with the increase of the reduction rate, the slip flat area of the rupture is increased obviously, while the number of shear dimples decreases. Notably, shear

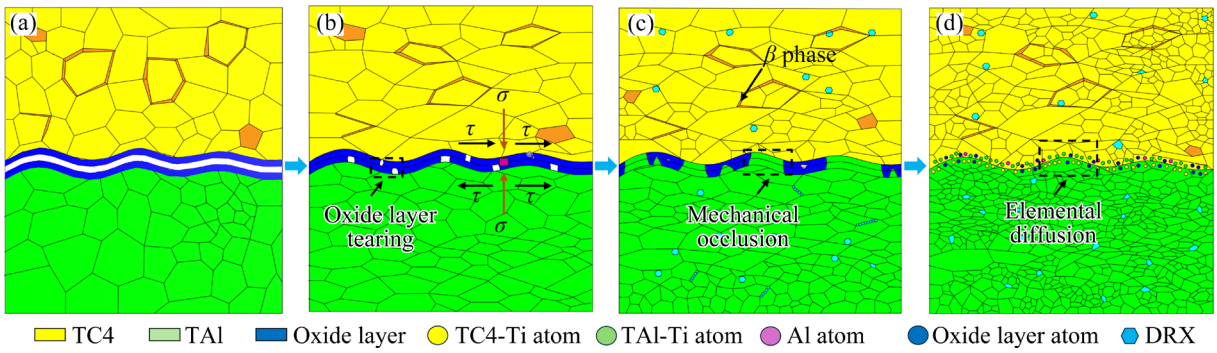

Fig. 15 Bonding schematic diagram of rolling process for TA1/TC4 composite plate: (a) Initial state; (b) Brittle layer fracture; (c) Mechanical occlusion; (d) Element diffusion

fracture of the composite plates with different reduction rates occurs in the TA1 matrix, which results in high interface bonding strength. It is shown that the interfacial shear strength of the composites is determined by the shear strength of the TA1 matrix.

Microstructural analysis reveals distinct differences between tensile and tensile−shear. The tensile fracture surface is displayed as isometric dimples, while the tensile−shear fracture is characterized by shear dimples. The microscopic morphology of the fracture is closely correlated with the stress triaxiality. In the tensile experiment, the material is subjected to normal tensile stress, with stress triaxiality ratio exceeding 1/3. The fracture mode is tensile fracture, characterized by the formation of equiaxed ductile dimples on the fracture surface. In contrast, during the tensile−shear experiment, the material is subjected to the combined effect of tensile and shear stresses at the bonding interface, as the stress triaxiality approaches zero. Therefore, the fracture mode is dominated by shear fracture, characterized by the formation of shear dimples along the shear direction on the fracture surface.

Figure 15 illustrates the bonding mechanism diagram of TA1/TC4 composite plate during rolling. At the beginning of rolling, there is a thin layer of brittle oxide on the surface of the plate. When the plates enter the backward slip zone, under the action of rolling and friction force, the brittle layer on the surface is increasingly split. Furthermore, fresh metal is extruded and the grains near the interface are elongated. After entering the sticking zone, the increase of interfacial shear stress enables fresh metal to break through the oxide layer and contacting with each other. Element diffusion is gradually strengthened at the bonding interface, accompanied by grain refinement. Simultaneously, dynamically recrystallized grains gradually appear under the action of external force and temperature field. When the plate enters the forward slip zone, the brittle layer is completely torn. In addition, the degrees of element diffusion and solid solution reaction in both substrates are intensified. Finally, this results in the formation of continuous diffusion layer accompanied by grain refinement, which leads to the increase of interfacial bonding strength and the significant improvement of comprehensive mechanical performances.

4 Conclusions

(1) With the increase of the reduction rate, the interface bonding quality is improved. Interface bonding mechanism involves metallurgical connection caused by element diffusion without forming IMCs. Besides, the plastic deformation degree of the TA1 side changes slightly, but the deformation degree of the TC4 side is significantly increased. With the increase of reduction rate, there are bimodal basal T-type textures on the TC4 side and basal tilted texture on the TA1 side.

(2) Bonding performance of the composite plate can be improved by the CR process. Meanwhile, the bonding performance at the trough exhibits higher quality compared to the peak. The equivalent strain of the TC4 side corresponding to the CR process is higher than that of the FR process. The temperatures during the two pass rolling processes are both 700 °C which remains below both the β-transus temperature of TC4 alloy and the

β-phase transformation temperature (882 °C) of TA1, which avoids the formation of large β phase.

(3) The grains in both substrates of the composite plate are noticeably refined as the reduction rate increases. The TA1/TC4 composite plate prepared by the "CR+FR" rolling process, with the first pass rolling temperature of 700 °C and reduction rate of 44%, exhibits the highest tensile and shear strengths, which are 749 and 403.87 MPa, respectively. In addition, the breakage types are changed from purely ductile to ductile−brittle characteristics, with the elongation of the composite decreasing from 16% to 6.2%.

CRediT authorship contribution statement

Peng ZHANG: Conceptualization, Writing − Review & editing, Supervision, Funding acquisition; **Hao ZHAO:** Conceptualization, Methodology, Software, Writing − Review & editing, Data curation; **Jin-zhou ZHU:** Methodology, Software, Writing − Original draft, Data curation; **Tao WANG:** Writing − Review & editing, Formal analysis, Resources; **Zhong-kai REN:** Supervision, Validation, Resources; **Jian-chao HAN:** Supervision, Validation; **Wen-wen LIU:** Supervision.

Declaration of competing interest

The authors declare that they have no known competing financial interests or personal relationships that could have appeared to influence the work reported in this paper.

Acknowledgments

This work was supported by the National Natural Science Foundation of China (No. 52275362), and Natural Science Foundation of Shanxi Province, China (No. 202303021224002), and the Central Government Guides the Special Fund Projects of Local Scientific and Technological Development (Nos. YDZJSX2021A020, YDZJSX2022A023).

References

[1] DHIB Z, GUERMAZI N, KTARI A, GASPERINI M, HADDAR N. Mechanical bonding properties and interfacial morphologies of austenitic stainless steel clad plates [J]. Materials Science and Engineering: A, 2017, 696: 374−386.

[2] HOSSEINI S A, HOSSEINI M, MANESH H D. Bond strength evaluation of roll bonded bi-layer copper alloy strips in different rolling conditions [J]. Materials & Design, 2011, 32(1): 76−81.

[3] LEK J Y, BHOWMIK A, TAN A W Y, SUN Wen, SONG Xu, ZHAI Wei, BUENCONSEJO P J, LI Feng, LIU Er-jia, LAM Y M, BOOTHROYD C B. Understanding the microstructural evolution of cold sprayed Ti−6Al−4V coatings on Ti−6Al−4V substrates[J]. Applied Surface Science, 2018, 459: 492−504.

[4] LIU Zhu-bo, WANG Xin-yue, LIU Ming-shuo, LIU Yuan-ming, LIU Jiang-lin, IGNATOV A V, WANG Tao. Microstructure and mechanical behavior of Ti/Cu/Ti laminated composites produced by corrugated and flat rolling [J]. Transactions of Nonferrous Metals Society of China, 2022, 32(8): 2598−2608.

[5] OU Peng, CAO Zeng-qiang, RONG Ju, YU Xiao-hua. Molecular dynamics study on the welding behavior in dissimilar TC4-TA17 titanium alloys [J]. Materials, 2022, 15(16): 5606.

[6] SU Hang, LUO Xiao-bing, CHAI Feng, SHEN Jun-chang, SUN Xin-jun, LU Feng. Manufacturing technology and application trends of titanium clad steel plates [J]. Journal of Iron and Steel Research International, 2015, 22(11): 977−982.

[7] ZHAO Zhi-po, TANG Jun-rong, TARIQ N U H, LIU Hou-sheng, LIU Han-hui, REN Yu-peng, TONG Min, YIN Li-song, DU Hao, WANG Ji-qiang, XIONG Tian-ying. Effect of rolling temperature on microstructure and mechanical properties of Ti/steel clad plates fabricated by cold spraying and hot-rolling [J]. Materials Science and Engineering: A, 2020, 795: 139982.

[8] BAI Yu-liang, LIU Xue-feng. Interfacial reaction behavior of titanium/steel composite plate formed by cold-hot rolling [J]. Materials Characterization, 2023, 202: 113030.

[9] QI Zi-chen, YU Chao, XIAO Hong. Microstructure and bonding properties of magnesium alloy AZ31/CP-Ti clad plates fabricated by rolling bonding [J]. Journal of Manufacturing Processes, 2018, 32: 175−186.

[10] HA J S, HONG S I. Deformation and fracture of Ti/439 stainless steel clad composite at intermediate temperatures [J]. Materials Science and Engineering: A, 2016, 651: 805−809.

[11] LI Zhi-ming, SUN Yan-le, LAVERNIA E J, SHAN Ai-dong. Mechanical behavior of ultrafine-grained Ti−6Al−4V alloy produced by severe warm rolling: The influence of starting microstructure and reduction ratio [J]. Metallurgical and Materials Transactions A, 2015, 46(11): 5047−5057.

[12] YANG Ming, CHEN Dai-guo, ZHOU Hen, XU Jun-feng, MA Hong-hao, SHEN Zhou-wu, ZHANG Bing-yuan, TIAN Jie. Experimental and numerical investigation of microstructure and evolution of TiNi alloy/Q235 steel interfaces prepared by explosive welding [J]. Journal of Materials Research and Technology, 2021, 15: 5803−5813.

[13] MENG Tao, WANG Ri-chu, CAI Zhi-yong, YAO Ying-jun. Microstructure and properties of Cu matrix composites reinforced with surface-modified Kovar particles [J]. Transactions of Nonferrous Metals Society of China, 2024, 34(10): 3251−3264.

[14] CHEN Gang, LI Jin-tao, XU Guang-ming. Bonding process and interfacial reaction in horizontal twin-roll casting of steel/aluminum clad sheet [J]. Journal of Materials Processing Technology, 2017, 246: 1−12.

[15] LI Shun-qiang, SUN Guo-sheng, ZHANG Rui-sheng,

CHENG Xiao, LIU Ji-zi. Effect of heat treatment on microstructure and mechanical property of roll-bonded 1060/7N01/1060 laminates [J]. Transactions of Nonferrous Metals Society of China, 2024, 34(1): 94−107.

[16] BEYGI R, CARBAS R J C, BARBOSA A Q, MARQUES E A S, da SILVA L F M. A comprehensive analysis of a pseudo-brittle fracture at the interface of intermetallic of η and steel in aluminum/steel joints made by FSW: Microstructure and fracture behavior [J]. Materials Science and Engineering: A, 2021, 824: 141812.

[17] ZHANG Quan-ming, ZHANG Yong, ZHANG Zhi-mei. Effect of diffusion heat treatment on strength and microstructure of TC4/TA1 brazed joint [J]. Welding & Joining, 2012, 8: 30−34, 69. (in Chinese)

[18] LI Yan-xing, WANG Lin, ZHU Lei, LI Ying, YAN Zhi-wei, SONG Yu-chen, CHENG Xing-wang. Investigation of interfacial structure and dynamic mechanical behavior of titanium alloy laminated composites [J]. Journal of Materials Research and Technology, 2022, 21: 5111−5120.

[19] LI Ting, WANG Tao, LIU Wen-wen, HUANG Zhi-quan, JIANG Zheng-yi, HUANG Qing-xue. Hot-rolling process and properties of large thickness ratio Al/Mg/Al laminates [J]. Transactions of Nonferrous Metals Society of China, 2023, 33(12): 3625−3640.

[20] XING Tong, LIU Cui-rong, LIU Jie, CUI Hai-lian, HU Xiao-tong, CHU Zhi-bing, TUO Lei-feng. Investigation on the interface morphology of Mg/Al corrugated composite plate in the straightening process [J]. Materials, 2022, 15(13): 4383.

[21] WANG Tao, WANG Yue-lin, BIAN Li-ping, HUANG Qing-xue. Microstructural evolution and mechanical behavior of Mg/Al laminated composite sheet by novel corrugated rolling and flat rolling [J]. Materials Science and Engineering A, 2019, 765: 138318.

[22] LIU Yan-xiao, LIU Yuan-ming, WANG Zhen-hua, LIU Yan-ping, WANG Tao, HUANG Qing-xue. Stress analysis and microstructure evolution of Cu/Al composite plate during corrugated rolling [J]. Transactions of Nonferrous Metals Society of China, 2023, 33(5): 1460−1471.

[23] REN Xian-wei, HUANG Yuan-chun, LIU Yu, ZHANG Xie-yi, ZHAO Li-kai, ZHOU Wen-long. Through-thickness shear texture of the twin-roll cast AA6016 sheet after asymmetric rolling and its recrystallization behavior [J]. Journal of Materials Research and Technology, 2021, 10: 1323−1338.

[24] WANG Tao, GAO Xiang-yu, ZHANG Zhi-xiong, REN Zhong-kai, QI Yan-yang. ZHAO Jing-wei. Interfacial bonding mechanism of Cu/Al composite plate produced by corrugated cold roll bonding [J]. Rare Metals, 2021, 40(5): 1284−1293.

[25] LI Sha, LIU Xin-yang, JIA Yi, HAN Jian-chao, WANG Tao. Interface characteristics and bonding performance of the corrugated Mg/Al clad plate [J]. Materials, 2021, 14(16): 4412.

[26] LI Shuang, LI Lei, SOULAMI A, POWELL C A, MATHAUDHU S, DEVARAJ A, WANG Chong-min. In-situ observation of deformation twin associated sub-grain boundary formation in copper single crystal under bending [J]. Materials Research Letters, 2022, 10(7): 488−495.

[27] ZHANG Kai, SHAO Zhu-tao, DANIEL C S, TURSKI M, PRUNCU C, LANG Li-hui, ROBSON J, JIANG Jun. A comparative study of plastic deformation mechanisms in room-temperature and cryogenically deformed magnesium alloy AZ31 [J]. Materials Science and Engineering: A, 2021, 807: 140821.

[28] LI Sha, LUO Chao, BASHIR M, JIA Yi, HAN Jian-chao, WANG Tao. Interface structures and mechanical properties of corrugated + flat rolled and traditional rolled Mg/Al clad plates [J]. Rare Metals, 2021, 40(10): 2947−2955.

[29] LI Sha, LUO Chao, LIU Zhi-dong, ZHAO Jing-wei, HAN Jian-chao, WANG Tao. Interface characteristics and mechanical behavior of Cu/Al clad plate produced by the corrugated rolling technique [J]. Journal of Manufacturing Processes, 2020, 60: 75−85.

[30] YANG Hong-fu, HUANG Ren-song, ZHANG Ye-lin, ZHENG Shan-ju, LI Meng-nie, KOPPALA S, KEMACHEEVAKUL P, SANNAPANENI J. Effect of rolling deformation and passes on microstructure and mechanical properties of 7075 aluminum alloy [J]. Ceramics International, 2023, 49(1): 1165−1177.

[31] CHANG Yu-ling, CHEN Hong-sheng, ZHOU Jun, LIU Run-ai, NIE Hui-hui, WANG Wen-xin. Micro-nano interface structure and mechanical characteristics of thin wall Cu/Al composite tubes prepared by strong staggered spinning [J]. Materials Characterization, 2023, 206: 113405.

[32] LI Zhen-lun, SONG Ke, KANG Qing-xin, ZHOU Tong-xv, XV Xun-hu, ZHAN Li-qiang, WANG Guo-feng. Microstructure evolution during high temperature rolling and effect on the mechanical properties of TiBw/Ti65 composites with network structure [J]. Materials Characterization, 2024, 208: 113642.

[33] GUO Xiong-wei, REN Zhong-kai, CHAI Zhe, WANG Tao, HUANG Qing-xue. Research on microstructure and mechanical properties of TC4/304 clad plates by asymmetric rolling with local strong stress [J]. Materials Science and Engineering: A, 2024, 893: 146166.

[34] XIAO Hong, QI Zi-chen, YU Chao, XU Cheng. Preparation and properties for Ti/Al clad plates generated by differential temperature rolling [J]. Journal of Materials Processing Technology, 2017, 249: 285−290.

[35] WANG Wen-jing, TU Ying-ming, LIU Mo-han, LIU Xue-feng. Effect of inhomogeneous plastic deformation on the interfacial microstructure and properties of titanium/ stainless steel [J]. Journal of Materials Research and Technology, 2023, 24: 1240−1251.

[36] WANG Wen-bo, LIU Xiang-yu, XU Nuo, JING Zhi-cheng, XU Guo-jian, XING Fei. Effect of solution temperature on microstructure and properties of Ti6Al4V by laser-directed energy deposition [J]. Journal of Materials Engineering and Performance, 2023, 32(4): 1515−1528.

[37] KO U J, JAVADINEJAD H R, PARK K T, KWON N, KIM J H. Kinetic study of electrochemical deoxidation of commercially pure titanium in molten magnesium chloride [J]. Journal of Materials Science, 2023, 58(27): 11235−11251.

压下率对 TA1/TC4 复合板界面组织及力学性能的影响机理

张 鹏[1,2,3]，赵 浩[2,3,4]，朱锦州[1,3,4]，王 涛[2,3,4]，任忠凯[2,3,4]，韩建超[2,3,4]，刘文文[2,3,4]

1. 太原理工大学 材料科学与工程学院，太原 030024；
2. 太原理工大学 金属成形技术与重型装备全国重点实验室，太原 030024；
3. 太原理工大学 先进金属复合材料成形技术与装备教育部工程研究中心，太原 030024；
4. 太原理工大学 机械工程学院，太原 030024

摘 要：研究波纹轧制压下率对波纹轧制+平轧工艺制备的 TA1/TC4 板材显微组织和力学性能的影响，建立复合板波纹轧制有限元模型并对其进行验证。实验结果表明，结合界面处无明显缺陷和金属间化合物存在。首道次波纹轧制温度为 700 ℃，压下率为 44%时，复合板的拉伸强度和界面剪切强度分别达到 749 和 403.97 MPa。模拟结果表明，波纹轧制增加了 TC4 的塑性应变，并且在波谷处的压应力值较高。波纹轧制有利于界面结合，并且随着压下率的增大，复合板力学性能得到显著改善。

关键词：波纹轧制；TA1/TC4 复合板；压下率；界面显微组织；界面结合性能

(Edited by Xiang-qun LI)